

A Quasi-2-Layer Morphodynamic Model

Sergio Maldonado^{1†}, and Alistair G. L. Borthwick²

¹Department of Geophysics, Stanford University, Stanford, CA 94305, U.S.A.

²Institute for Energy Systems, School of Engineering, University of Edinburgh, The King's Buildings, Edinburgh EH9 3JL, U.K.

(Received xx; revised xx; accepted xx)

Conventional approaches to simulating morphodynamics in open channels often suffer from a high degree of empiricism, which translates into uncertainty in the final results. Here, we derive a model for predicting sediment transport rates and morphological evolution, based on previous models for two-layer-averaged shallow flows over erodible beds. A distinct feature of the present model is the treatment of the lower (bedload) layer as having constant, vanishing thickness, but variable (in time and space) average density. There is no requirement to use a particular empirical formula for sediment transport rates in order to achieve closure, and so the model reduces the level of empiricism inherent to most conventional approaches. The model is validated against popular empirical formulae for bedload and total load, and proves to conform with established bedload theory. The model provides estimates of the thickness of a sheet transport layer in agreement with previous approaches, predicts the cubic proportionality between bedload and depth-averaged flow velocity, and seemingly reconciles conflicting views on the behaviour of shear stress under sediment transport. By considering the benchmark case of a migrating submerged hump (or sandbar) subject to a steady current, it is found that the present model performs better than a conventional model in predicting the correct evolution of the hump while achieving model stability without further treatment.

Key words: No keywords required when submitting for revision.

1. Introduction

Most Conventional Morphodynamic (CM) models consist of a coupled system of hydrodynamic equations (e.g. the Shallow Water Equations), a bed-update equation (e.g. Exner equation), and a sediment-transport formula. A feature common to virtually all CM models is dependency on empirical or semi-empirical formulae for the estimation of sediment transport rates. However, the vast number of such formulae available in the literature makes selection of the most appropriate expression difficult in practice, leading to considerable uncertainty. Although some research has focused on the inter-comparison of sediment transport formulae (see e.g. Gomez & Church 1989; Yang & Wan 1991; Camenen & Larroude 2003; Van Emelen *et al.* 2015), the findings from such investigations converge to the common conclusion that there is no best or universal expression. Different formulae perform better than others depending on the particular conditions to be simulated, which may be anticipated given the specific laboratory setting under which such formulae were derived. For example, typical degrees of

† Email address for correspondence: sergiomv@stanford.edu

accuracy in bedload empirical formulae fall within a factor of 5-10 (Amoudry & Souza 2011). Furthermore, studies have shown that the final morphological results can be very sensitive to the selection of a particular sediment transport expression (e.g. Garnier *et al.* 2006; Dissanayake *et al.* 2009), which is why the high degree of empiricism involved in the estimation of sediment transport rates is recognised as a major source of uncertainty in CM models (Amoudry & Souza 2011). Moreover, sediment transport in coastal and river environments is typically divided into bedload and suspended load. Although different mechanisms govern these two modes of transport, an objective criterion to distinguish one from the other has yet to be provided (Fredsoe & Deigaard 1992). For example, bedload is often defined as the mode of transport taking place in the *vicinity* of the bed; however, a reliable method to determine the thickness of the bedload layer does not exist (except for the particular case of sheet flow, where a distinct transport layer can be identified). Therefore, ambiguity in the identification of the mode of transport present (i.e. bedload vs suspended load) is reflected in the selection of an appropriate type of formula, thus adding to uncertainty. Further unreliability in CMMs also arises from lack of understanding about the fundamental mechanics behind sediment transport. In particular, accurate prediction of initiation of sediment motion remains a longstanding challenge to the scientific community, partly due to the complexity involved in the near-bed hydrodynamics of open channels.

Alternatives to the CM models described above include two-phase (e.g. Bakhtyar *et al.* 2009; Greco *et al.* 2013), and two-layer models, which are mutually similar in their conceptualisation of the phenomenon, complexity, and computational performance. The earliest approaches to morphodynamics by means of 2-layer models are due to Capart & Young (1998) and Fraccarollo & Capart (2002) who investigated sheet flow caused by dam-break-induced erosion of the bed. Fraccarollo & Capart (2002) introduced the idea of an erosion rate estimated using simple concepts borrowed from open channel hydraulics and soil mechanics, thus replacing some of the empiricism inherent to the typical estimation of sediment transport with physical mechanisms behind bed erosion. Fraccarollo & Capart's conceptualisation of the flow consisted of clear water flowing on top of a constant-density sediment-water-mixture, which in turn had the same average density as the non-mobile bed underneath; both fluid layers moved at the same speed. Later, Spinewine (2005) extended Fraccarollo & Capart's model to account for different velocities and concentrations in both fluid layers (a study of the impact of such an enhancement is given by Zech *et al.* 2008); the average density of the transport layer, however, continued to be treated as constant. The latter restriction was recently removed by Li *et al.* (2013), who considered a variable-density lower layer; nonetheless, Li *et al.* still required an empirical formula for sediment transport rates in order to predict the variability in density. All the aforementioned models simulate clear water over a transport layer, and assume a distinct physical interface dividing both layers.

Here, we derive a quasi-2-layer model for sediment transport and morphological evolution, which idealises shallow water-sediment flow as being divided into two layers with temporally varying densities; however, the thickness of the lower (bedload) layer is fixed. The model deals naturally with the ambiguity in the distinction between modes of transport (it is weakly dependent on the arbitrarily set thickness of the lower layer) and does not require the selection of a particular sediment-transport formula, hence reducing the degree of empiricism, and thus uncertainty, common to most CM models.

The paper is organised as follows. §2 presents the derivation of the model and underlying

assumptions. §3 describes use of the model for conditions where no sediment is transported permitting comparison against results from standard 1-layer-averaged hydrodynamic models. In §4, bedload is considered, allowing the model to be tested against different theoretical aspects of bedload, and validated against widely employed empirical expressions for bedload. In §5, the model is also validated against empirical formulae for total load (i.e. bedload and suspended transport). §6 examines the case of an erodible migrating submerged hump subject to a steady current. §7 summarises the key findings.

2. Model description

2.1. Assumptions

We idealise the water-sediment mixture as being divided into two layers: the lower concerned with bedload transport, and the upper representing sediment in suspension. The water-sediment mixture is assumed to be an incompressible continuum, with each layer experiencing zero vertical acceleration such that the flow is hydrostatic and essentially two-dimensional, being predominantly in the horizontal plane. Uniform sediment size is considered. This paper deals solely with the 1D version of the model. Uniform horizontal velocities (u) and sediment concentrations (c) are assumed within each of the two layers (see Figure 1); these velocities and concentrations can vary both in time and space. The bedload layer is treated as having constant, arbitrary, vanishing thickness and variable density. This permits simulation of the, often ambiguously defined, bedload layer as a near-bed transport zone, whose sediment density can vary from zero for no sediment transport, to a maximum or saturation value. The interface dividing the lower and upper layers is treated as an imaginary line rather than as a sharp physical interface or discontinuity in density. The present model is referred to as a Quasi-2-Layer (Q2L) model, in order to distinguish it from typical 2-Layer models representing a stratified flow consisting of two layers with different but constant, homogeneous densities (e.g. Fraccarollo & Capart 2002; Spinewine 2005; Zech *et al.* 2008), where the interface between layers does correspond to a physical discontinuity in average densities.

The model is intended to simulate three different modes of transport:

- Mode 0: no sediment transport. For flow conditions below the threshold of sediment motion, both layers consist of pure water (Figure 1.b).
- Mode 1: bedload only. Flow conditions are such that only the lower layer carries sediment and the upper layer consists of pure water (Figure 1.c).
- Mode 2: total load. At higher flow conditions, the bedload layer has reached a saturation point and sediment entrains into the upper layer, where it is treated as suspended load (Figure 1.d).

The assumed vertical structures of the fluid velocity and concentration profiles are closer to the observed vertical distributions in real channels than those of a single-layer model. The vertical profile of sediment concentration (e.g. Figure 1.d) reproduces accurately the occurrence of the maximum concentration in the near-bed zone (see e.g. Pugh & Wilson 1999). The vertical velocity distribution (Figure 1.a) also gives a closer representation of the near-bed (boundary layer) hydrodynamics. The distribution can potentially represent events where different parts of the fluid column move in opposite directions (e.g. potentially during backwash and uprush on a beach).

It is assumed that the fluid is always in motion, encompassing low speed hydrodynamic

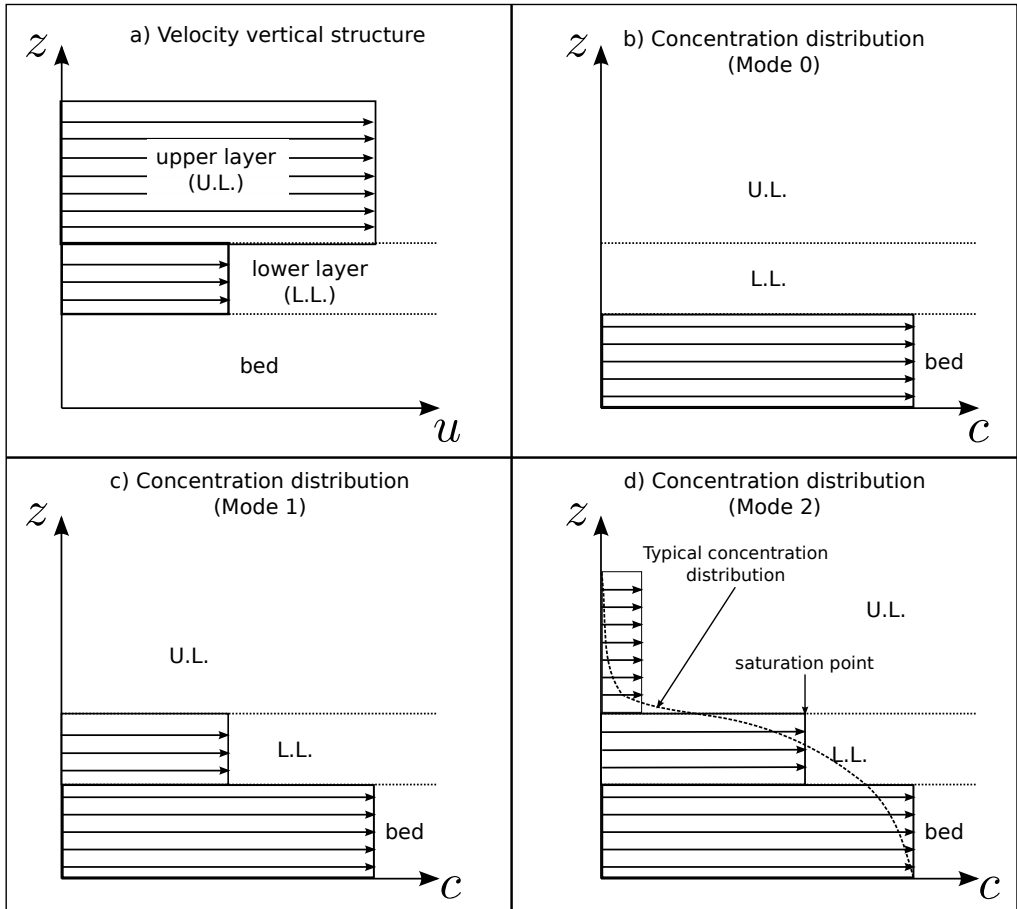


FIGURE 1. Assumed vertical structures for velocity and concentration: a) vertical structure of the fluid horizontal velocity; b), c) and d), vertical distribution of the sediment concentration for transport Modes 0, 1 and 2, respectively.

conditions below the threshold of sediment motion (Mode 0), and higher speed flow where the velocity is sufficient to incorporate sediment into the lower layer (Mode 1) and eventually into the upper layer (Mode 2). Certain cases not modelled include still fluid, sediment being present in the upper layer when the lower one has not reached saturation point (due perhaps to an external source of sediment), and sudden entrainment caused by intense turbulence (e.g. due to a breaking wave) or an adjacent source of sediment (e.g. in a river). Sheet-flow transport, where a distinct interface occurs between the lower transport layer and the upper pure-water layer, can be simulated by the present model (as Mode 1). The well-defined sheet-layer thickness may not coincide with the arbitrarily set bedload layer thickness, but the overall sediment transport rate may nevertheless be accurately predicted by the model (see §4.3). Flows carrying highly concentrated suspended loads are also outside the scope of the present model, noting that different approaches (e.g. Fang & Wang 2000; Rosatti & Fraccarollo 2006) may be required in order to explain inherent phenomena, such as the minimum concentration occurring just above the bed instead of near the free surface (Ni *et al.* 2000). Fine cohesive sediments are not considered given their different transport mechanics (i.e. once they are eroded by relatively fast flows, they are carried in suspension without necessarily going through

the bedload stage).

To simulate entrainment and deposition, the sediment erosion rate (a negative value corresponds to deposition) is estimated from the conservation of horizontal momentum at the bed interface, which is related in turn to the difference between the time-averaged shear stress exerted by the fluid on the bed surface and the effective bed resistance (more details in §2.2.2).

2.2. Governing equations

2.2.1. Derivation

The model comprises mass and momentum conservation laws for a fluid vertically divided into 2 layers over an erodible bed, supplemented by empirical formulae for interface and bed shear stresses. The following derivation of the governing equations commences from the classical 2-Layer Shallow Water Equations (Abbott 1979), after which certain assumptions are reviewed/imposed and source terms defined. The 1D 2-Layer Shallow Water Equations are written in their generic form (modified from Abbott 1979) as follows:

$$\frac{\partial(\rho_1 h_1)}{\partial t} + \frac{\partial(\rho_1 h_1 u_1)}{\partial x} = i^{(i)} \quad (2.1a)$$

$$\frac{\partial(\rho_0 h_0)}{\partial t} + \frac{\partial(\rho_0 h_0 u_0)}{\partial x} = -i^{(i)} \quad (2.1b)$$

$$\frac{\partial(\rho_1 h_1 u_1)}{\partial t} + \frac{\partial}{\partial x} \left(\rho_1 h_1 u_1^2 + \frac{1}{2} \rho_1 g h_1^2 \right) + \rho_1 g h_1 \frac{\partial(h_0 + z_b)}{\partial x} = j^{(i)} \quad (2.1c)$$

$$\frac{\partial(\rho_0 h_0 u_0)}{\partial t} + \frac{\partial}{\partial x} \left(\rho_0 h_0 u_0^2 + \frac{1}{2} \rho_0 g h_0^2 \right) + g h_0 \left[\frac{\partial(\rho_1 h_1)}{\partial x} + \rho_0 \frac{\partial z_b}{\partial x} \right] = j^{(b)} - j^{(i)} \quad (2.1d)$$

where subscripts ‘0’ and ‘1’ refer to the lower and upper layers, L_0 and L_1 , respectively; ρ , h and u are the layers’ density, depth and depth-averaged horizontal velocity, respectively; g denotes gravitational acceleration; z_b is the bed level with respect to a fixed horizontal datum (subscript b refers to the bed layer, L_b); and i and j represent net mass and momentum exchanges between layers (taken as positive in the upward direction) through the interfaces denoted by the superscripts (i) and (b) . See Figure 2 for reference. Term $i^{(i)}$ represents the mass exchange between upper and lower layers when inter-layer fluxes take place; $j^{(i)}$ and $j^{(b)}$ then comprise the net vertical fluxes of horizontal momentum through interfaces (i) and (b) , respectively, resulting from mass exchanges and interface shear stresses. For a fixed bed, $j^{(b)}$ can be converted into a bed shear stress. Note that the assumption of uniform velocity profiles implies a Boussinesq profile coefficient equal to unity, which should otherwise be present in the momentum-conservation equations. A similar remark applies to the case of concentration profiles; i.e. a uniform (fully mixed) profile, in conjunction with a uniform velocity, implies a profile factor equal to unity, which in another case should be included in the mass-conservation equations. Equations (2.1a) to (2.1d) are the governing equations of a system consisting of a shallow stratified flow over a fixed bed.

The Q2L morphodynamic model incorporates mass and momentum exchanges between the bed (L_b) and the fluid layer above it (L_0), not considered in (2.1). Net mass exchange takes place through interface (b) and is added as a source term to eq. (2.1b), leading to its right-hand side becoming: $i^{(b)} - i^{(i)}$. This mass exchange yields a change in the bed elevation, z_b , and so an equation governing the bed evolution is also added. Conservation

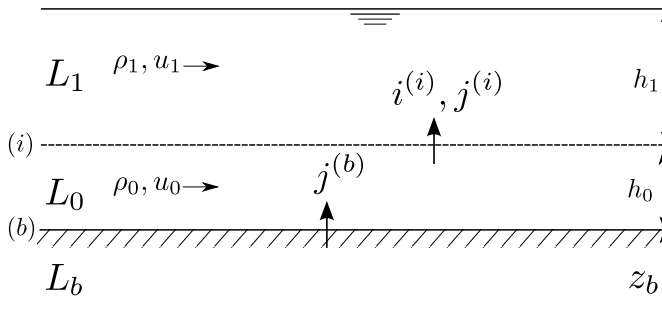


FIGURE 2. Definition sketch for the classical 2-Layer Shallow Water Equations.

of overall mass in the bed layer, L_b , gives:

$$\frac{\partial(\rho_b z_b)}{\partial t} = -i^{(b)}, \quad (2.2)$$

where ρ_b is the bed average density. Assuming constant ρ_b , the above equation becomes:

$$\frac{\partial z_b}{\partial t} = -e^{(b)}, \quad (2.3)$$

where $e^{(b)} = i^{(b)}/\rho_b$ is the net volumetric exchange between layers L_b and L_0 .

A further assumption (key to the present model) is that the thickness of the lower layer can be treated as a constant in space and time, such that

$$\frac{\partial h_0}{\partial t} = \frac{\partial h_0}{\partial x} = 0. \quad (2.4)$$

This reduces the third term on the left-hand side of (2.1c) to $\rho_1 g h_1 \partial z_b / \partial x$, and also leads to a revised version of eq. (2.1b). Consider steady flow below the threshold of motion (no sediment transport, hence $\rho_0 = \rho_1 = \rho_w$), such that a horizontal gradient of the lower-layer water flow velocity exists in part of the domain (i.e. $\partial u_0 / \partial x \neq 0$). In this case, (2.1b) can be written as:

$$\rho_w \frac{\partial h_0}{\partial t} + h_0 \frac{\partial \rho_0}{\partial t} + u_0 \frac{\partial(\rho_w h_0)}{\partial x} + \rho_w h_0 \frac{\partial u_0}{\partial x} = 0. \quad (2.5)$$

Invoking (2.4), eq. (2.5) yields $\partial \rho_0 / \partial t = -\rho_0 \partial u_0 / \partial x$, and so the model would predict a change in density within the lower layer (since $\partial \rho_0 / \partial t \neq 0$) even for conditions below the threshold of sediment motion. For this reason, eq. (2.1b) has to be replaced by an equation representing the conservation of *sediment* mass within the lower layer, namely:

$$\frac{\partial(\rho_s c_0 h_0)}{\partial t} + \frac{\partial(\rho_s c_0 h_0 u_0)}{\partial x} = i_s^{(b)} - i_s^{(i)}, \quad (2.6)$$

where i_s denotes net exchange of sediment mass through a given interface, and c_0 is the sediment concentration in L_0 . Note that (2.6) implies that sediment particles transported in the bedload layer move at the same stream-wise velocity as the whole water-sediment mixture. In other words, $u_{s0} = u_0$ is assumed, where u_{s0} represents the bedload particles' stream-wise velocity. Such an assumption may differ from observations; however, use of a Lagrangian model for particle saltation in the near-bed area, reveals that when $u_{s0} = u_0$ is assumed, the final outputs of the model (i.e. sediment transport rates and morphological evolution) remain virtually unaffected (see Appendix A). Therefore, this paper pragmatically assumes equivalence between the sediment particle stream-wise

velocity and the velocity of the corresponding water-sediment-mixture, unless otherwise explicitly stated. Conservation of sediment mass within the upper layer leads to:

$$\frac{\partial(\rho_s c_1 h_1)}{\partial t} + \frac{\partial(\rho_s c_1 h_1 u_1)}{\partial x} = i_s^{(i)}, \quad (2.7)$$

where c_1 is the sediment concentration in the upper layer. As before, (2.7) assumes $u_{s1} = u_1$, where u_{s1} is the stream-wise velocity of sediment particles in L_1 . Note that this assumption is more sensible than $u_{s0} = u_0$, given that for suspended load, sediment is expected to be transported by the current at roughly the same speed of the flow (Soulsby 1997).

In summary, the Quasi-2-Layer morphodynamic model in 1D, depicted schematically in Figure 3, is thus defined by the following set of governing equations:

$$\frac{\partial(\rho_1 h_1)}{\partial t} + \frac{\partial(\rho_1 h_1 u_1)}{\partial x} = i^{(i)} \quad (2.8a)$$

$$\frac{\partial(\rho_s c_1 h_1)}{\partial t} + \frac{\partial(\rho_s c_1 h_1 u_1)}{\partial x} = i_s^{(i)} \quad (2.8b)$$

$$\frac{\partial(\rho_s c_0 h_0)}{\partial t} + \frac{\partial(\rho_s c_0 h_0 u_0)}{\partial x} = i_s^{(b)} - i_s^{(i)} \quad (2.8c)$$

$$\frac{\partial(\rho_1 h_1 u_1)}{\partial t} + \frac{\partial}{\partial x} \left(\rho_1 h_1 u_1^2 + \frac{1}{2} \rho_1 g h_1^2 \right) + \rho_1 g h_1 \frac{\partial z_b}{\partial x} = j^{(i)} \quad (2.8d)$$

$$\frac{\partial(\rho_0 h_0 u_0)}{\partial t} + \frac{\partial}{\partial x} \left(\rho_0 h_0 u_0^2 + \frac{1}{2} \rho_0 g h_0^2 \right) + g h_0 \left[\frac{\partial(\rho_1 h_1)}{\partial x} + \rho_0 \frac{\partial z_b}{\partial x} \right] = j^{(b)} - j^{(i)} \quad (2.8e)$$

$$\frac{\partial z_b}{\partial t} = -e^{(b)} \quad (2.8f)$$

The set of governing equations (2.8), corresponds to the conservation of: overall water-sediment mass in the upper layer (2.8a); sediment mass in the upper layer (2.8b); sediment mass in the lower layer (2.8c); overall water-sediment horizontal momentum in the upper layer (2.8d); overall water-sediment horizontal momentum in the lower layer (2.8e); and sediment mass in the bed (2.8f).

2.2.2. Erosion rate and shear stresses

The erosion rate (with deposition negative) is estimated as a function of the difference between the shear stress exerted by the fluid on the bed and the bed resistance, and the velocity jump between bed interface (see Fraccarollo & Capart 2002; Spinewine 2005); namely:

$$e^{(b)} = \frac{1}{\rho_b |u_0|} (\tau_0^{(b)} - \tau_b^{(b)}), \quad (2.9)$$

where $\tau_0^{(b)}$ and $\tau_b^{(b)}$ represent the shear stress exerted by the fluid on the bed surface and the bed resistance, respectively. As stated in §2.1, the present idealisation assumes a fluid always in motion; however, should $u_0 = 0$ occur at some point in the domain

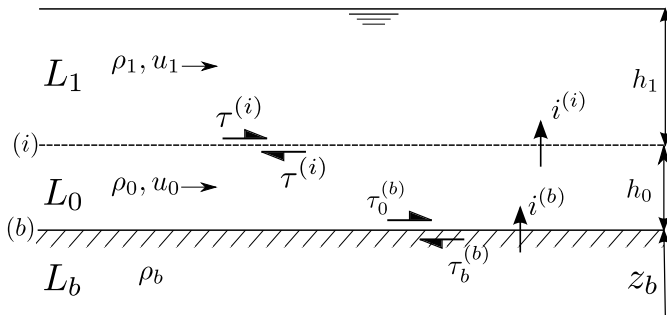


FIGURE 3. Definition sketch for the Quasi-2-Layer model.

at a certain time, the condition $e^{(b)} = 0$ for $u_0 = 0$ is imposed in order to avoid a mathematical error. Equation (2.9) derives from conservation of longitudinal momentum across the bed discontinuity (Spinewine 2005).

Herein, $\tau_0^{(b)}$ is estimated using a Chézy-type expression dependent on the squared velocity slip at the bed interface (b) and the bedload layer average density, ρ_0 ; namely:

$$\tau_0^{(b)} = c^{(b)} \rho_0 |u_0| u_0, \quad (2.10)$$

where $c^{(b)}$ is a drag coefficient, one of the main calibration parameters within the present model. By making $\tau_0^{(b)}$ dependent on ρ_0 (as opposed to the density of water, ρ_w), the influence is incorporated of the skin-friction and sediment-transport contributions to the total bed shear stress. The effect of bed-surface features (e.g. ripples) could be represented by modifying accordingly the coefficient $c^{(b)}$, following the conventional approach.

The bed interface is treated as a failure plane, and so the shear stress $\tau_b^{(b)}$ can be related to Terzaghi's effective normal stress, $\sigma'^{(b)}$, through Coulomb's law, which describes the stress state at failure for a rigid granular assembly as (Spinewine 2005):

$$\tau_b^{(b)} = \tau_c + \sigma'^{(b)} \tan \varphi, \quad (2.11)$$

where τ_c is the critical yield stress, obtained from Shields' curve, and φ is the soil friction angle, assumed equal to the angle of repose. The effective normal stress, $\sigma'^{(b)}$, is evaluated as the difference between the normal stress just beneath the bed interface assuming hydrostatic pressure, $\sigma^{(b)}$ ($= \rho_0 g h_0 + \rho_1 g h_1$), and the pore water pressure at the bed, $p_w^{(b)}$ ($= \rho_w g (h_0 + h_1)$). Hence, $\sigma'^{(b)} = \sigma^{(b)} - p_w^{(b)}$, or:

$$\sigma'^{(b)} = [h_1(\rho_1 - \rho_w) + h_0(\rho_0 - \rho_w)]g; \quad (2.12)$$

thus, allowing the bed resistance to be expressed in its generic form as:

$$\tau_b^{(b)} = \{\tau_c + [h_1(\rho_1 - \rho_w) + h_0(\rho_0 - \rho_w)]g \tan \varphi\} |u_0| / u_0, \quad (2.13)$$

where the term $|u_0| / u_0$ is included in order to ensure that $\tau_b^{(b)}$ acts as a resistive stress oriented in the direction opposite to the flow (as defined in Figure 3). Spinewine (2005) and Fraccarollo & Capart (2002) provide comprehensive descriptions of the methodology and assumptions underpinning the derivation of shear stresses and erosion rate functions stated above.

Note that estimation of shear stresses at interface (b) (i.e. $\tau_0^{(b)}$ and $\tau_b^{(b)}$) represent the main source of empiricism in this model. Nevertheless, as will be proved later, the degree of empiricism involved in the present model is significantly lower than that of conventional morphodynamic models, given that the Q2L model does not require the selection of a particular empirical expression for computing sediment transport rates. In general, both shear stresses, $\tau_0^{(b)}$ and $\tau_b^{(b)}$, acting on the bed interface should be taken purely as auxiliary variables used to help quantify accurately the erosion rate, $e^{(b)}$, and associated sediment transport rate and bed evolution (primary aims of the present model).

For L_1 , the interface shear stress, $\tau^{(i)}$, can be treated as a bed resistance (Abbott 1979), which in turn acts on L_0 as a driving stress (analogous to the free-surface interface in a wind-driven flow), with equal magnitude but opposite direction (see Figure 3). Although the shear stress at interface (i) is single-valued, an exchange of mass can take place between both layers (L_0 and L_1) as detailed in §2.3. A Chézy-type expression provides a simple way to estimate $\tau^{(i)}$, which is also consistent with the assumed vertical structure of the flow; namely:

$$\tau^{(i)} = c^{(i)} \rho_1 |u_1 - u_0| (u_1 - u_0), \quad (2.14)$$

where $c^{(i)}$ is a second calibration coefficient, the first being $c^{(b)}$ in eq. (2.10).

2.3. Inter-layer fluxes

Consider the case of initiation of sediment motion (Mode 1) depicted in Figure 4. Assumption of constant h_0 (i.e. constant volume of L_0) implies that when the *water-sediment* mass mixture is eroded from the bed at a rate $i^{(b)}$, an equal volume of *water* has to be exchanged between L_0 and L_1 for the volume of L_0 to remain constant. For simplicity (though not necessarily correct from a phenomenological perspective), this can be viewed as follows: when eroded from the bed, the immersed volume of water-sediment mixture pushes an equal volume of water in L_0 up to L_1 (see Figure 4). Hence, for bedload transport only (i.e. c_0 below the maximum permitted value, $c_{0\text{mx}}$), for a given mass flux through interface (b), $i^{(b)}$, there is a corresponding mass flux through interface (i), such that:

$$i^{(i)} = \rho_w e^{(b)}, \quad (2.15)$$

where ρ_w is the density of water. Spinewine (2005) provides an alternative explanation for a similar exchange of water between fluid layers when bed erosion takes place, using Reynolds' concept of granular dilatancy. It should be noted however that the present analysis differs from that of Spinewine (2005), who assumed the density of L_0 constant, unlike the volume. The water exchange $i^{(i)}$ ensures that the free surface, $\eta = z_b + h_0 + h_1$, remains constant under uniform steady conditions when only bedload transport occurs (i.e. $c_0 \neq 0$ and $c_1 = 0$).

For total transport (Mode 2), L_0 saturates and sediment enters L_1 as suspended load. Given that the saturated L_0 cannot incorporate any more sediment, the mass flux of eroded bed material has to be compensated by the same water-sediment mass flux between the fluid layers through interface (i). Hence, for the case of total transport (where $c_0 = c_{0\text{mx}}$ and $c_1 \geq 0$):

$$i^{(i)} = i^{(b)} = \rho_b e^{(b)}. \quad (2.16)$$

For flow conditions below the threshold of sediment motion (Mode 0), $\tau_0^{(b)} < \tau_b^{(b)}$ and

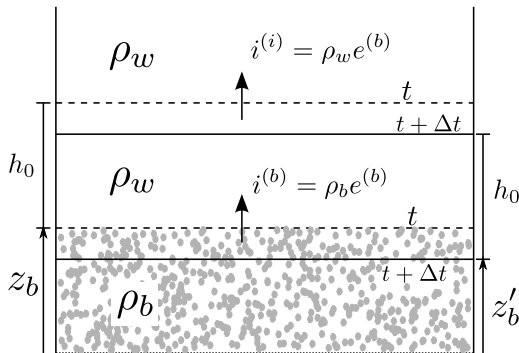


FIGURE 4. Sketch illustrating the initiation of erosion. Horizontal dashed(continuous) lines represent the instant immediately before(after) erosion takes place. z'_b denotes the new bed level (at $t + \Delta t$).

$\tau_b^{(b)} = \tau_c$ by definition, yielding $e^{(b)} < 0$, which would predict deposition even when no sediment is available to be deposited by the flow (i.e. $c_0 = c_1 = 0$). To avoid this, the following condition is imposed:

$$i^{(i)} = i^{(b)} = 0, \quad \text{if } e^{(b)} < 0 \quad \text{and} \quad c_0 = c_1 = 0, \quad (2.17)$$

In summary, the net mass fluxes through interfaces (b) and (i) are expressed as:

$$i^{(b)} = \begin{cases} 0 & \text{if } e^{(b)} < 0 \quad \text{and} \quad c_0 = c_1 = 0 \\ \rho_b e^{(b)} & \text{else} \end{cases} \quad (2.18)$$

and

$$i^{(i)} = \begin{cases} 0 & \text{if } i^{(b)} = 0 \\ \rho_w e^{(b)} & \text{if } c_0 \neq 0 \quad \text{and} \quad c_1 = 0 \\ \rho_b e^{(b)} & \text{if } c_0 = c_{0\text{mx}} \quad \text{and} \quad c_1 \geq 0 \end{cases} . \quad (2.19)$$

The corresponding *sediment* mass fluxes are the sediment components of the total water-sediment mass exchanges, expressed as:

$$i_s^{(b)} = c_b \frac{\rho_s}{\rho_b} i^{(b)}, \quad (2.20)$$

and

$$i_s^{(i)} = \begin{cases} 0 & \text{if } c_0 < c_{0\text{mx}} \quad \text{and} \quad c_1 = 0 \\ c_b \rho_s e^{(b)} & \text{if } c_0 = c_{0\text{mx}} \quad \text{and} \quad c_1 \geq 0 \end{cases} . \quad (2.21)$$

Exchange of horizontal momentum between layers takes place when mass crosses the interface from one layer to an adjacent layer. This occurs at both interfaces (i) and (b) when $i^{(b)} \neq 0$ (and hence $i^{(i)} \neq 0$). For $i^{(i)} > 0$ ($i^{(i)} < 0$), L_1 experiences gain(loss) in momentum equivalent to the magnitude of the mass crossing (i) multiplied by the original horizontal velocity, i.e. $u_0(u_1)$. In other words:

$$j_c^{(i)} = \begin{cases} i^{(i)} u_0 & \text{if } i^{(i)} > 0 \\ i^{(i)} u_1 & \text{if } i^{(i)} < 0 \end{cases}, \quad (2.22)$$

where subscript c denotes the convective or geomorphic component of the overall momentum transfer, j . The other part is the resistive shear stress, which can be considered as a frictional or diffusive momentum exchange, j_d (Spinewine 2005). Hence, $j = j_c + j_d$. For interface (i):

$$j_d^{(i)} = -\tau^{(i)}. \quad (2.23)$$

Note that the assumption of $\tau^{(i)}$ acting on both sides of interface (i) with equal magnitude but opposite direction, implies that a gain(loss) of convective momentum experienced by L_1 yields a loss(gain) in L_0 of convective momentum of the same magnitude. This is not necessarily true for layers L_0 and L_b . Unlike interface (i), interface (b) experiences different shear stresses, $\tau_0^{(b)}$ and $\tau_b^{(b)}$, on its upper and lower sides. However, at the interface, the total momentum exchange $j^{(b)}$ has to be single-valued. For this reason, $j^{(b)}$ can be computed based on variables from both sides; namely:

$$j^{(b)} = j_c^{(b)} + j_d^{(b)} = \begin{cases} i^{(b)} u_0 - \tau_0^{(b)} \\ i^{(b)} u_b - \tau_b^{(b)} = -\tau_b^{(b)} \end{cases}, \quad (2.24)$$

where u_b is the bed horizontal velocity, which is equal to zero by definition. Frictional momenta (shear stresses) necessarily act as diffusive terms either side of the interface. It should be noted that both expressions stated in (2.24) are mathematically equivalent when either erosion or deposition take place (i.e. $e^{(b)} \neq 0$); however, the first formulation is adopted within the model for convenience, for the following reason. Under no-sediment-transport conditions (Mode 0; $e^{(b)} = 0 \Rightarrow j_c^{(b)} = 0$), L_0 faces solely a resistive bed friction proportional to the square of its velocity ($j^{(b)} = j_d^{(b)} \propto u_0^2$). This behaviour is not predicted by $j^{(b)} = -\tau_b^{(b)}$ given that, from eq. (2.13), $\tau_b^{(b)} = \tau_c = \text{constant}$, for conditions below the threshold of motion. However, the first formulation for $j^{(b)}$ in (2.24) does replicate this behaviour; invoking eq. (2.10), for $e^{(b)} = 0 (\Rightarrow i^{(b)} = 0)$, $j^{(b)} = -\tau_0^{(b)} = c^{(b)} \rho_0 |u_0| u_0$ (thus, $j^{(b)} = j_d^{(b)} \propto u_0^2$). Hence, the overall momentum exchange through interface (b) is evaluated as:

$$j^{(b)} = i^{(b)} u_0 - \tau_0^{(b)}. \quad (2.25)$$

Combining (2.22) and (2.23), the overall momentum transfer through (i) is given by:

$$j^{(i)} = \begin{cases} i^{(i)} u_0 - \tau^{(i)} & \text{if } i^{(i)} > 0 \\ i^{(i)} u_1 - \tau^{(i)} & \text{if } i^{(i)} < 0 \end{cases}. \quad (2.26)$$

Equations (2.25), (2.26), (2.18)-(2.21), and shear stresses defined by (2.10), (2.13) and (2.14) close the set of governing equations given by (2.8).

3. No sediment transport (Mode 0)

The no-sediment-transport case allows comparison to be made between the present model and a conventional 1-layer SWE-based hydrodynamic model. A methodology is now developed to calibrate the Q2L model based purely on hydrodynamic information. Steady uniform flow over an inclined non-erodible channel is considered. A fixed bed, or

flow below the threshold of sediment motion, implies the following: $e^{(b)} = 0 \Rightarrow i^{(b)} = i^{(i)} = 0$; $\partial z_b / \partial t = 0$; $\partial h_1 / \partial t = 0$; $\rho_0 = \rho_1 = \rho_w$ (i.e. $c_0 = c_1 = 0$); $j^{(b)} = -\tau_0^{(b)}$; $j^{(i)} = -\tau^{(i)}$. By imposing the condition of uniform steady and unidirectional flow, and after some algebraic manipulation, a relation between the two main calibration parameters $c^{(b)}$ and $c^{(i)}$ can be obtained, namely:

$$\frac{c^{(b)}}{c^{(i)}} = \frac{h_T}{h_1} \left(\frac{u_1}{u_0} - 1 \right)^2, \quad (3.1)$$

where $h_T = h_0 + h_1$ is the total channel depth. Rewriting the above equation as $u_1/u_0 = [(h_1 c^{(b)}) / (h_T c^{(i)})]^{1/2} + 1$ indicates that $u_1 > u_0$, as expected. In a single-layer depth-averaged hydrodynamic model, the bed resistance, τ , is usually calculated from the expression $\tau = c_f \rho_w \bar{u}^2$; where c_f is the bed friction coefficient, and \bar{u} is the flow horizontal velocity averaged over the whole depth. Noting that $\tau = \tau_0^{(b)} = c^{(b)} \rho_w u_0^2$ (for no-sediment-transport conditions), then:

$$\frac{c^{(b)}}{c_f} = \left(\frac{\bar{u}}{u_0} \right)^2, \quad (3.2)$$

which illustrates the non-equivalence between the friction coefficients $c^{(b)}$ and c_f , given that $u_1 > u_0 \Rightarrow \bar{u} > u_0 \Rightarrow c^{(b)} > c_f$. It is important to interpret $c^{(b)}$ as a particular bed-friction indicator within the Q2L model, without confusing $c^{(b)}$ with c_f , which is typically a function of a Chézy or Manning coefficient. For the assumed velocity distributions, \bar{u} relates to the Q2L model variables h_0 , h_1 , u_0 and u_1 through

$$\bar{u} = \frac{u_0 h_0 + u_1 h_1}{h_0 + h_1}. \quad (3.3)$$

For a given open channel flow, if there are available data on the vertical structure of the fluid horizontal velocity component, $u(z)$, then depth-averaged velocities u_0 and u_1 , corresponding to a given h_0 and h_1 , can be calculated. This information can then be utilised to tune parameters $c^{(b)}$ and $c^{(i)}$ using eqs. (3.1) to (3.3). For illustrative purposes, two expressions are considered for predicting the horizontal velocity profile. The first expression, proposed by Yang *et al.* (2004), is a log-law-based equation designed for smooth uniform open channel flows. The second, proposed by Soulsby (1997), is intended for use in tidal (hydrodynamically rough) currents. These expressions have been selected in order to study a wider range of values of the ratio h_1/h_0 . Figure 5 depicts the ratios $c^{(b)}/c_f$ and $c^{(b)}/c^{(i)}$ as functions of h_1/h_0 , for the two velocity profiles. Both velocity-profile formulations exhibit congruent behaviour. Coefficients $c^{(b)}$ and c_f are of similar orders of magnitude; in fact, $c^{(b)}/c_f \in [4, 6]$ covers a wide range of practical applications. Estimation of the bed drag coefficient, c_f , depends on the average flow velocity, hydraulic radius and bed roughness; typical values of c_f are in the range of 10^{-3} to 10^{-2} (Soulsby 1997). Fig. 5 also shows that $c^{(i)} \sim c^{(b)}$; whereas in practice, $c^{(b)} > c^{(i)}$ is anticipated. The foregoing demonstrates that the Q2L model can be calibrated without considering sediment transport, provided information on $u(z)$ is available. Values of $c^{(b)}/c_f$ and $c^{(b)}/c^{(i)}$ depicted in Fig. 5 should be taken only as a guide, noting they have been computed for particular velocity-profile formulations. Strictly speaking, the momentum equations within the present model should account for the vertical non-uniformity of the velocity profile through Boussinesq profile coefficients or dispersion stresses. However, for uniform flow (considered herein) the non-linear terms in the equations affected by the profile-correction coefficients are zero, and so the present

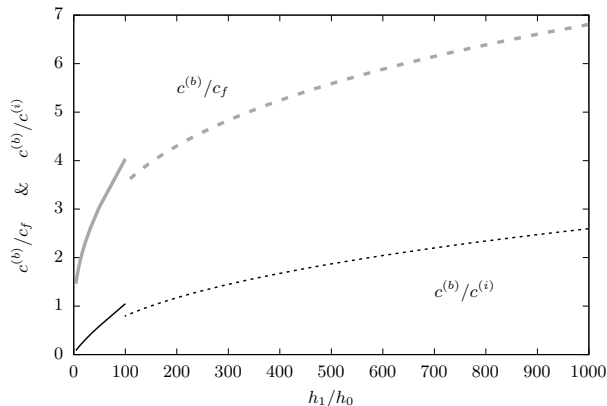


FIGURE 5. Ratios $c^{(b)}/c_f$ (thick gray lines) and $c^{(b)}/c^{(i)}$ (thin black lines) as functions of h_1/h_0 for velocity profiles given by Yang *et al.* (2004) (continuous lines) and Soulsby (1997) (dashed lines).

analysis remains valid.

4. Bedload transport (Mode 1)

We now consider steady uniform flow over an erodible bed with bedload transport ($c_0 \leq c_{0\text{mx}}$ and $c_1 = 0$). This case permits derivation of analytical solutions to the Q2L model, which can then be used to compare the present model against bedload theory, including validation against empirical formulae.

4.1. Analytical solution

The volumetric bedload transport rate, q_b , is evaluated from:

$$q_b = h_0 c_0 u_0 . \quad (4.1)$$

Note that the *sediment* bedload rate should strictly be computed as $q_b = h_0 c_0 u_{s0}$. However, this would require an additional equation relating u_{s0} to the model output u_0 . Appendix A proves that the assumption $u_0 \approx u_{0s}$ appears sensible from quantitative and pragmatic perspectives. For steady uniform flow that is initially above the threshold of sediment motion, equilibrium conditions for sediment transport are expected to be reached eventually. Given that h_0 is a constant within the present model, equilibrium-state values have to be found solely for c_0 and u_0 in order to compute q_b . Once bed erosion has initiated, steady sediment transport conditions can only occur once $e^{(b)}$ decreases to zero. This happens when both c_0 and u_0 have reached certain values ($c_{0\text{eq}}$ and $u_{0\text{eq}}$), such that the force exerted by the water-sediment flow on the bed surface equals its resistance to erosion. Recall the equation governing bed erosion, eq. (2.9). For $e^{(b)} = 0$ to occur, $\tau_0^{(b)} = \tau_b^{(b)}$ has to be verified. Hence, $\tau_0^{(b)} = \tau_b^{(b)} \Rightarrow \tau_0^{(b)} = \tau_c + (\rho_0 - \rho_w)h_0g \tan \varphi$; from which an expression for the equilibrium bedload layer density can be found, namely:

$$\rho_{0\text{eq}} = \frac{\tau_0^{(b)} + \rho_w g h_0 \tan \varphi - \tau_c}{g h_0 \tan \varphi} . \quad (4.2)$$

The bedload layer equilibrium concentration, $c_{0\text{eq}}$, is related to $\rho_{0\text{eq}}$ through $c_{0\text{eq}} =$

$(\rho_{0\text{eq}} - \rho_w) / (\rho_s - \rho_w)$; thus:

$$c_{0\text{eq}} = \frac{\tau_0^{(b)} - \tau_c}{(\rho_s - \rho_w)gh_0 \tan \varphi}. \quad (4.3)$$

From the definition of $\tau_0^{(b)} (= \rho_0 c^{(b)} u_0^2)$, the equilibrium flow speed in the bedload layer, $u_{0\text{eq}}$, is given by:

$$u_{0\text{eq}} = \left(\frac{\tau_0^{(b)}}{\rho_{0\text{eq}} c^{(b)}} \right)^{1/2}. \quad (4.4)$$

Hence, the bedload transport rate, equal to $h_0 c_{0\text{eq}} u_{0\text{eq}}$, is:

$$q_b = \frac{(\tau_0^{(b)} - \tau_c)}{(\rho_s - \rho_w)g \tan \varphi} \left(\frac{\tau_0^{(b)}}{\rho_{0\text{eq}} c^{(b)}} \right)^{1/2}. \quad (4.5)$$

Equation (4.5) provides a straightforward way of estimating the bedload transport rate as function of bed shear stress, sediment characteristics (ρ_s , D and τ_c) and a tuning parameter $c^{(b)}$. Note that bedload is then independent of the second calibration parameter $c^{(i)}$.

4.2. Mathematical agreement with bedload formulae

Inspection of (4.5) reveals that the bedload transport rate predicted by the present model follows the general form:

$$q_b = A' \left(\tau_0^{(b)} - \tau_c \right) \left(\tau_0^{(b)} \right)^{1/2}, \quad (4.6)$$

where $A' = [(\rho_s - \rho_w)g \tan \varphi]^{-1} (\rho_{0\text{eq}} c^{(b)})^{-1/2}$. This is in agreement with several empirical and semi-empirical bedload formulations (e.g. Bagnold 1963; Nielsen 1992; Soulsby 1997; Yalin 1963), which can be written, in non-dimensional form, as $\Phi = F(\theta - \theta_c) \theta^{1/2}$, where Φ , θ and θ_c are non-dimensional bedload transport, bed shear stress and critical Shields parameter, respectively; and F is a non-dimensional expression (often taken as a constant obtained from a best-fit curve to laboratory data). In Appendix A, it is shown that by computing bedload as $q_b = h_0 c_{0\text{eq}} u_{s0}$, and relating u_{s0} to u_0 by means of Lagrangian simulations, q_b follows the form $q_b = A'(\tau - \tau_c)(\hat{d}\tau^{1/2} - \hat{c}\tau_c^{1/2})$ (where \hat{c} and \hat{d} are calibration coefficients), which is also in agreement with various empirical expressions (e.g. Madsen 1991; Ashida & Michue 1972).

Sheet flow is considered to be a special case of bedload transport that takes place at relatively fast flows, when $\theta \gg \theta_c$; approximately at $\theta \equiv \tau/g(\rho_s - \rho_w)D > 0.8$ (Nnadi & Wilson 1992; Soulsby & Damgaard 2005). During this transport regime, bed forms are washed out if initially present and sediment is transported within a well-defined layer a few millimetres thick. The transport rate under sheet-flow conditions can be described satisfactorily as being dependent on the flow velocity cubed (Ribberink & Al-Salem 1994; Capart & Young 1998); i.e. $q_b \propto \bar{u}^3$. For sheet flow, $\tau_0^{(b)} \gg \tau_c \Rightarrow \tau_0^{(b)} - \tau_c \approx \tau_0^{(b)}$. Under these conditions, eq. (4.5) can be rewritten as:

$$q_b = \frac{1}{(\rho_{0\text{eq}} c^{(b)})^{1/2} (\rho_s - \rho_w)g \tan \varphi} \left(\tau_0^{(b)} \right)^{3/2} = \frac{\rho_{0\text{eq}} c^{(b)}}{(\rho_s - \rho_w)g \tan \varphi} u_0^3. \quad (4.7)$$

From eq. (3.2), it is observed that u_0 and the whole-depth averaged velocity \bar{u} exhibit

a linear relationship; hence $q_b \propto \bar{u}^3$, confirming consistency between the present model and sheet-flow theory. Furthermore, an analysis similar to that of Fraccarollo & Capart (2002) can be undertaken. For $\tau_c \approx 0$, the erosion rate can be expressed as:

$$e^{(b)} = \frac{1}{\rho_b u_0} \left(\tau_0^{(b)} - \tau_b^{(b)} \right) = \frac{1}{t_l} \left(M u_0^2 - \frac{\rho_0 - \rho_w}{\rho_0} h_0 \right), \quad (4.8)$$

where $M = c^{(b)}/(g \tan \varphi)$ is a mobility parameter; and $t_l = \rho_b u_0 / (\rho_0 g \tan \varphi)$ is a lag time related to the inertia of sediment accelerated from rest to the sheet flow velocity (when erosion takes place). This is consistent with the view that sediment transport does not respond immediately to changes in bed shear stress, but instead has a characteristic time of relaxation (Parker *et al.* 2003). This relaxation time is often neglected (under the assumption of instantaneous response of a sediment particle to the imposed shear stress) without serious consequences for slow morphological changes; however, the time lag is significantly important for fast morphological changes. The term $(\rho_0 - \rho_w)h_0/\rho_0$ can be related to the transport capacity of the sheet layer. Similar quantities have been found within the framework of alluvial hydraulics and dam-breaks (e.g. Armanini & Di Silvio 1988; Fraccarollo & Capart 2002).

4.3. Sheet layer thickness

The sheet layer thickness, δ_{sh} , is estimated from the vertical force balance of particles in the sheet layer, assuming the vertical distribution of the sediment concentration within the layer to vary linearly from a maximum equal to c_b , to zero at the sheet-layer surface (Fredsoe & Deigaard 1992). This leads to (Soulsby & Damgaard 2005):

$$\delta_{\text{sh}} = \frac{2(\tau - \tau_c)}{c_b(\rho_s - \rho_w)g \tan \varphi_d}, \quad (4.9)$$

where $\tan \varphi_d$ is the coefficient of dynamic friction, and $c_b/2$ is taken to be the average concentration of the sheet layer. Note that the equation for $c_{0 \text{ eq}}$ given by (4.3) is consistent with (4.9). The present model assumes varying density within a fixed layer defined by h_0 . However, δ_{sh} can be estimated from the Q2L model by fixing $c_{0 \text{ eq}}$ for sheet-flow conditions ($0.21 \lesssim c_{0 \text{ eq}} \lesssim 0.25$, according to Spinewine 2005) and then solving (4.3) for h_0 , yielding:

$$\delta_{\text{sh}} \approx h_0 = \frac{(\tau_0^{(b)} - \tau_c)}{c_0(\rho_s - \rho_w)g \tan \varphi}. \quad (4.10)$$

Note that (4.10) equals (4.9) provided $c_0 = c_b/2$ and $\tan \varphi = \tan \varphi_d$. The first proviso is perfectly justified given that both c_0 and $c_b/2$ represent the average concentration of the sheet layer. The second proviso is also reasonable (Kovacs & Parker 1994). A linear relationship between the sheet layer thickness and bed shear stress has also been reported by Wilson (1987) and Capart & Young (1998).

4.4. The ‘shield’ effect

According to Fernández Luque & van Beek (1976), the bedload layer (L_0) acts as a ‘shield’ that prevents the upper water layer (L_1) from further eroding the bed. Bagnold (1956) suggested the same and argued that this was due to the fluid component of the bed shear stress being reduced to the value of τ_c at the bed surface by the presence of particles in the bedload layer. However, this theory has been criticised (see e.g. Fernández Luque & van Beek 1976; Niño & García 1998; Parker *et al.* 2003; Seminara *et al.* 2002), especially for low concentrations of particles within the bedload layer. Here, we show that the

present model conforms with both sets of views without contradiction. For equilibrium bedload conditions, the model requires $\tau_0^{(b)} = \tau_b^{(b)}$. Here, $\tau_b^{(b)} (= \tau_c + \sigma'^{(b)} \tan \varphi)$ can be interpreted as a ‘critical’ bed shear stress in the Bagnoldian sense, hence agreeing with Bagnold’s intuitive idea of a fluid-induced stress (in this case, the fluid is a water-sediment continuum) being reduced to a critical value in order for erosion to cease. Moreover, for a natural steady uniform flow (where $S_b < 0$, with $S_b = \partial z_b / \partial x$ being the bed-slope), it can readily be shown from the governing equations that: $\tau^{(i)} - \tau_0^{(b)} = -\rho_0 g h_0 S_b > 0$, leading to:

$$\tau^{(i)} > \tau_0^{(b)} > \tau_c. \quad (4.11)$$

This implies that the bedload layer indeed acts as a ‘shield’ whereby the (water) fluid shear stress at the top of the bedload transport layer $\tau^{(i)}$ is reduced to a ‘critical’ value $\tau_0^{(b)}$ at the bed surface, which in turn is larger than τ_c . Note that $\tau_0^{(b)}$ represents the shear stress exerted by the sediment-water mixture defining the bedload layer, and not exclusively the water fluid shear stress. However, for low values of c_0 such that $\rho_0 \approx \rho_w$, $\tau_0^{(b)}$ can be taken as the fluid component of the bed shear stress, in agreement with Fernández Luque & van Beek (1976). Furthermore, the erosion rate $e^{(b)}$ is associated to a *net* transfer of mass between the bed and the bedload layer, so that the condition $e^{(b)} = 0$ required for steady transport represents a dynamic, rather than static, state. This agrees with the view that simultaneous entrainment and deposition of sediment take place under steady conditions (Fernández Luque & van Beek 1976; Parker *et al.* 2003). It may be therefore concluded that the current model reconciles (or least is not in contradiction with) the conceptualisations of bed shear stress in the presence of bedload described by Bagnold and those of his critics.

4.5. On Exner equation

Conservation of sediment mass within layers L_b (the static bed) and L_0 (the bedload layer) yields the following expression:

$$\frac{\partial z_b}{\partial t} + \xi h_0 \frac{\partial c_0}{\partial t} + \xi \frac{\partial q_b}{\partial x} = 0, \quad (4.12)$$

where $\xi = 1/c_b$ is related to bed porosity. If the term $\xi h_0 \partial c_0 / \partial t$ is neglected, the above equation is the same as the popular Exner equation (i.e. $\partial z_b / \partial t + \xi \partial q_b / \partial x = 0$). Such a term is however related to the adaptation time required for the accelerating/decelerating sediment particles crossing the interface (b) between layers with different velocities (i.e. L_b and L_0), and can thus be neglected solely in certain circumstances. For steady or quasi-steady sediment transport conditions, $\partial c_0 / \partial t \approx 0$ can be assumed, and (4.12) becomes the Exner equation. Nevertheless, for problems involving fast morphological changes (e.g. due to a dam break), the term $\partial c_0 / \partial t$ may not be negligible (see e.g. Fraccarollo & Capart 2002). Moreover, equation (4.12) highlights the importance of understanding the Exner equation as representing conservation of sediment mass in the bed *and* the bedload transport layer above it. It is common to find in the literature references to the Exner equation as denoting conservation of sediment *in the bed*, which may yield confusing (even erroneous) interpretations of results under certain scenarios. For example, in the context of fast morphological changes induced by the break of a dam, a model based on the Exner equation may yield the misleading conclusion that a morphological bore –manifesting itself as a raised elevation of the bed level– propagates downstream along with the driving hydraulic bore. However, in reality a scour hole is produced by the hydraulic bore, and so the apparent raised bed elevation predicted by

an Exner-based model would result from misinterpreting the active bedload layer as part of the static bed.

4.6. Validation against formulae

Fig. 6 compares the model predictions (eq. 4.6) against empirical bedload formulae by Meyer-Peter & Müller (1948) (MP & M), Yalin (1963) (Y), Ashida & Michue (1972) (A & M), Wilson (1966) (W), Nielsen (1992) (N) and Fernández Luque & van Beek (1976) (FL & vB). These empirical formulae have been selected because they do not require any additional assumptions (e.g. value of bed-friction coefficient), other than the sediment characteristics (used to compute τ_c). Two particle diameters are considered: 0.5 and 2.0 mm. These particle sizes represent medium-coarse and very coarse sands, respectively, according to the Wentworth grain size scale. Coarse sand is considered here because bedload is expected to be the main mode of transport for $D > 0.3$ mm (Soulsby & Damgaard 2005). The parameters values are $s = 2.65$ and $\varphi = 32.1^\circ$; $h_0 = 10D$. The arbitrarily set h_0 is analysed later. Three values of $c^{(b)}$ are investigated; namely, 0.01, 0.03 and 0.06.

Predictions by the present model fall within the band of estimates delimited by the empirical formulae considered; this band illustrates the well-known uncertainty in the quantification of bedload. This adherence to the selected empirical formulae confirms the mathematical agreement with such expressions (as previously discussed). Model predictions are truncated where $c_0 = c_{0\text{mx}}$ is reached (here $c_{0\text{mx}} = 0.3$). Values of the bed-drag coefficient (for 1-layer models) typically fall in the range of $10^{-3} \lesssim c_f \lesssim 10^{-2}$, and so the middle value $c^{(b)} = 0.03$ is in agreement with the values of the ratio $c^{(b)}/c_f$ derived in §3 (see Fig. 5). For example, a value of $c^{(b)}/c_f \approx 4$ would yield $c_f \approx 7.5 \times 10^{-3}$, implying relatively rough hydrodynamic flow. Flows over beds composed of coarse sands such as considered herein can be treated as hydrodynamically rough, and so these findings validate both the ability of the present model to simulate bedload and the predictions of the ratio $c^{(b)}/c_f$ undertaken previously, based solely on hydrodynamic (i.e. no sediment transport) considerations.

Comparison between Figures 6(a) and 6(b) demonstrates that the overall behaviour of the Q2L model in relation to established empirical formulae is independent of the particle size within the range considered. The recommended value of $c^{(b)}$ depends on the reference formula. For flow conditions well above incipient motion, $c^{(b)} = 0.01$ yields close agreement between the present model and formulations by Yalin (1963), Ashida & Michue (1972), Wilson (1966) and Nielsen (1992); $c^{(b)} = 0.06$ leads to a better match with the expression by Fernández Luque & van Beek (1976); and for the middle value of $c^{(b)} = 0.03$, the model results are closer to those from the formula by Meyer-Peter & Müller (1948). Based on the present empirical equations, the range of $0.01 \leq c^{(b)} \leq 0.06$ can be taken as a suggested operational range when calibrating the Q2L model.

4.7. Bedload layer thickness, h_0

A reliable method to determine the thickness of the bedload layer does not exist. In the present model, the layer L_0 (defined by h_0) is used to represent the bedload zone. Fig. 7 investigates the sensitivity of the bedload predicted by the model to values of h_0 in the range of $[2D, 20D]$. This range is selected noting estimates of bedload layer thickness by Einstein (1950) and van Rijn (1984a). The particle diameter is 1.0 mm. The influence of the arbitrary h_0 on the predicted q_b , for a given $\tau_0^{(b)}/\tau_c$, is small. For

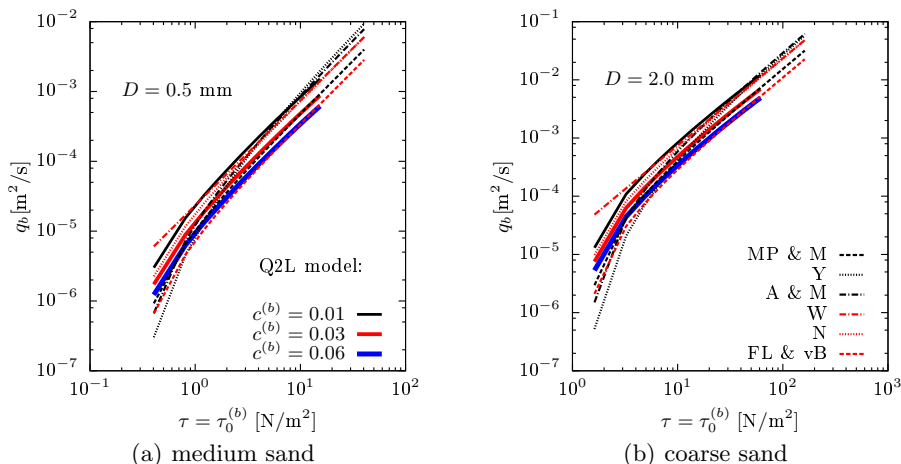


FIGURE 6. Comparison between dimensional bedload rates as functions of bed shear stress predicted by the Q2L model (continuous lines) against some empirical and semi-empirical expressions (broken lines), for two particle diameters. [Acronyms defined in corresponding paragraph; see §4.6]

$\tau_0^{(b)}/\tau_c = 20$ (where sheet flow is expected), the discrepancies between the curves are negligible. The most significant effect of the selected value of h_0 is the variation in the range of validity of the model when operating as Mode 1. The curves are plotted up to the point where $c_0 = c_{0\text{max}} = 0.3$, beyond which sediment is transported as suspended load (Mode 2) within the framework of the present model. A larger value of h_0 allows the model to operate as Mode 1 over a wider range of $\tau_0^{(b)}$.

Consider now eq. (4.9) to determine the thickness of a sheet layer, rewritten here as:

$$\frac{\delta_{\text{sh}}}{D} = \frac{2(\theta - \theta_c)}{c_b \tan \varphi_d}, \quad (4.13)$$

where non-dimensionalisations $\theta \equiv \tau/g(\rho_s - \rho_w)D$ and $\theta_c \equiv \tau_c/g(\rho_s - \rho_w)D$ have been employed. An alternative criterion to set the thickness of L_0 is to select a value of h_0 that ensures $h_0 \geq \delta_{\text{sh}}$ when sheet flow is simulated. In other words, if the maximum expected values of θ is known *a priori*, h_0 should be selected so as to meet the condition $h_0 \geq \delta_{\text{sh}}$, with δ_{sh} estimated from (4.13). This would ensure that the Q2L model treats the sheet flow as bedload (Mode 1), and not as bedload plus suspended load (Mode 2). For example, assuming standard values of $\tan \varphi_d \approx 0.65$, $\theta_c \approx 0.05$ and $c_b/2 \approx 0.3$, eq. (4.13) varies linearly from $[(\delta_{\text{sh}}/D)|_{\theta/\theta_c=1}] = 0$ to $[(\delta_{\text{sh}}/D)|_{\theta/\theta_c \approx 50}] \approx 10$. Therefore, $h_0 = 10D$ would ensure sheet flow is treated as bedload by the model for conditions up to $\tau_0^{(b)} \approx 50\tau_c$ (note, from Fig. 7, that Mode 1 is valid up to $\tau_0^{(b)} \approx 60\tau_c$ for $h_0 = 10D$). Hence $h_0 \approx 10D$ is recommended given the relatively wide range of validity yielded for Mode 1. The value $h_0 = 10D$ is used hereinafter as a default unless otherwise stated.

5. Total transport (Mode 2)

For sufficiently fast flows, particles will become entrained as suspended load into the upper fluid layer transporting sediment well above the near-bed zone, which when added

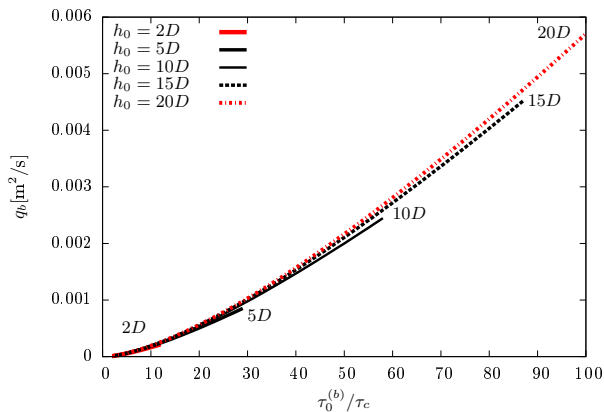


FIGURE 7. Predicted bedload vs non-dimensional bed shear stress (or transport stage) for different values of h_0 .

to the bedload, constitutes the total load. We now consider a scenario where the bedload layer has reached saturation and sediment becomes entrained into the upper layer L_1 . As with bedload, the assumption of steady uniform flow over a flat erodible bed permits the derivation of an analytical solution.

5.1. Analytical solution

Formulae for total transport typically depend on channel physical parameters (e.g. h_T , D). For the purpose of comparison, an analytical solution is now derived as a function of typical channel parameters using the present model. Total transport is computed by summation of bedload and suspended load,

$$q_T = q_b + q_s, \quad (5.1)$$

where q_T and q_s represent total and suspended loads. Here, $q_b(q_s)$ represents the sediment transported in layer $L_0(L_1)$. Equilibrium bedload is calculated considering that L_0 has reached its maximum transport capacity; in other words:

$$q_{b \text{ eq}} = q_b|_{c_0=c_{0\text{mx}}} = h_0 c_{0\text{mx}} u_0|_{c_0=c_{0\text{mx}}}. \quad (5.2)$$

Analogous to bedload, suspended load is computed as the product $h_1 c_{1\text{eq}} u_{1\text{eq}}$. The implicit assumption of $u_1 = u_{1s}$ is again justified given the fast flows associated with suspended load, which transport sediment at practically the same speed as the carrying fluid. Uniform steady unidirectional flow is considered in order to derive expressions for the equilibrium values of c_1 and u_1 . Following the previous methodology, equilibrium sediment transport conditions are achieved when $\tau_0^{(b)} = \tau_b^{(b)}$. Suspended transport normally occurs at flow velocities well beyond the threshold of motion, and so $\tau_c = 0$ is assumed. It also assumed that $h_1 \gg h_0$, so that the flux of water from L_0 to L_1 due to bed erosion is neglected, yielding $h_1 = \text{constant}$. The governing equations (2.8) then lead to: $\rho_{1\text{eq}} \approx [\rho_w h_T \tan \varphi - h_0 \rho_{0\text{mx}} (\tan \varphi + S_b)] / [h_1 (\tan \varphi + S_b)]$. Noting that $c_1 = (\rho_1 - \rho_w) / (\rho_s - \rho_w)$, then

$$c_{1\text{eq}} \approx \frac{h_0 \tan \varphi - h_1 S_b - h_0 (\rho_{0\text{mx}} / \rho_w) (\tan \varphi + S_b)}{(s-1) h_1 (\tan \varphi + S_b)}. \quad (5.3)$$

Conservation of momentum in the upper layer (eq. 2.8d) reduces to $\tau^{(i)} =$

$c^{(i)} \rho_{1\text{eq}} (u_{1\text{eq}} - u_0)^2 = -\rho_{1\text{eq}} g h_1 S_b$, yielding:

$$u_{1\text{eq}} = u_{0\text{eq}} + \left(\frac{-g h_1 S_b}{c^{(i)}} \right)^{1/2}, \quad (5.4)$$

where $u_{0\text{eq}} = u_0|_{c_0=c_{0\text{mx}}}$ is estimated from (2.8e), namely:

$$u_{0\text{eq}} = u_0|_{c_0=c_{0\text{mx}}} = \left[\frac{-g S_b}{c^{(b)}} \left(h_0 + \frac{\rho_w}{\rho_{0\text{mx}}} h_1 \right) \right]^{1/2}. \quad (5.5)$$

Employing equations (5.3)-(5.5), the total transport can be computed as:

$$q_T = h_0 c_{0\text{mx}} u_{0\text{eq}} + h_1 c_{1\text{eq}} u_{1\text{eq}}. \quad (5.6)$$

5.2. Validation against empirical formulae

For validation purposes, we select two empirical expressions for total transport presented by Engelund & Hansen (1967) and van Rijn (1984b), owing to their wide use and because they were originally applied to steady flows in rivers. Herein: $h_T = 10$ m; $D = 0.2$ mm (uniform sediment); $h_0 = 10D$ (hence, $h_1 \gg h_0$ is verified); and $c_{0\text{mx}} = 0.25$. Inspection of the analytical solution reveals that the present model requires two tuning parameters for total load; namely, $c^{(b)}$ and $c^{(i)}$. The additional degree of freedom for calibration (with respect to the case of bedload only) can be removed by proposing a value for the ratio $c^{(b)}/c^{(i)}$ based on hydrodynamic considerations. In §3, a methodology is proposed for estimating $c^{(b)}/c^{(i)}$ as a function of h_1/h_0 given a velocity profile. Noting that $h_1/h_0 \approx 5,000$, and assuming that the current follows the velocity profile described by Soulsby (1997), a value of $c^{(b)}/c^{(i)} = 5$ is prescribed. Model calibration for bedload has been carried out in §4.6 (see Fig. 6), where it is suggested that $0.01 \leq c^{(b)} \leq 0.06$. Fig. 8 compares predictions obtained by the selected empirical formulae and the present model for values of $c^{(b)} = 0.05, 0.056, 0.06$ and $c^{(b)}/c^{(i)} = 5$. It can be seen that the present model fits the formula by Engelund & Hansen (1967) better than that of van Rijn (1984b). In fact, for $c^{(b)} = 0.056$, the agreement between the model prediction and Engelund & Hansen's formula is outstanding over the range of parameters studied. Note that the discrepancy between estimates from the two empirical expressions can reach a factor of 2 (and this factor may increase when other empirical formulae, such as that of Ackers & White 1973, are included in the comparison). This level of uncertainty is unlikely to be improved upon significantly, given that inter-comparison of empirical data exhibits a similar degree of accuracy (Soulsby 1997). At low velocities, the agreement between the model and both formulae is satisfactory. At fast flows, discrepancies become relevant.

If the ratio $c^{(b)}/c^{(i)}$ cannot be determined from hydrodynamic considerations (for example, due to lack of information or reliable assumptions about the velocity profile), and both $c^{(b)}$ and $c^{(i)}$ are tuned independently, tests conducted demonstrate that the model predictions can fit satisfactorily those of van Rijn (1984b) (figure not shown for brevity). Therefore, if no reliable information is available on the flow hydrodynamics, no conclusions can then be drawn regarding which empirical expression yields the best agreement with the present model. Under such circumstances, the model should be calibrated directly against data for sediment transport rates. However, for practical applications, in the absence of hydrodynamic and sediment transport information, our recommendation is to assume a standard velocity profile and then follow the methodology described in §3 in order to estimate the ratio $c^{(b)}/c^{(i)}$. Fig. 5 can be used as a first approximation for rough hydrodynamic and relatively deep flows (e.g. tidal flows).

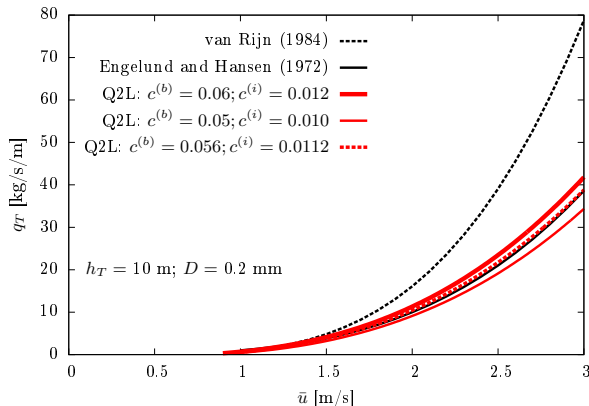


FIGURE 8. Comparison between the Q2L model predictions and empirical estimates of total sediment transport as function of flow average velocity. Three values of $c^{(b)}$ are considered; the ratio of $c^{(b)}/c^{(i)} = 5$ is fixed.

6. Case study: a migrating hump

The case of a submerged erodible hump (or sandbar) subject to a steady subcritical flow offers a simple, informative benchmark study for morphological models, and has been extensively analysed by researchers (e.g. Castro Díaz *et al.* 2008; Huang *et al.* 2008; Hudson & Sweby 2003; Johnson & Zyserman 2002). An initially symmetrical hump migrates in the stream-wise direction and its downstream face (lee) steepens with time. Here, we compare hump evolution profiles predicted by the Q2L model and a Conventional Morphological (CM) model. The latter represents the basic structure of conventional 2DH morphological models widely used in coastal and river engineering, which consists of coupled hydrodynamic, bed morphologic, and sediment-transport equations. In this case, the CM model comprises a coupled version of the 1D Shallow Water Equations, the Exner bed-update equation and a bedload equation applicable to sheet flow given by $q_b = B\bar{u}^3$, where B is a constant dependent on sediment and flow characteristics. The Q2L and CM models are solved numerically with second-order central differences in space and fourth-order Runge-Kutta integration in time. The following parameters are considered: channel length, $l = 1000$ m; $B = 0.001$ s²/m; $\xi = 1/0.6$ (bed porosity equal to 0.4, or $c_b = 0.6$); channel inclination of -0.006° ; water depth at the upstream boundary, $h_u = 10$ m and discharge per unit width, $Q = 10$ m²/s. For the Q2L model, three additional parameters are required: $D = 2.0$ mm; $h_0 = 10D$; and $c^{(b)} = 0.02$.

Fig. 9 shows the predictions of evolved hump profiles at different times for both models. When the CM model is employed, instabilities develop in the form of high-frequency oscillations at the crest and base of the upstream face (stoss) of the hump. These instabilities grow with time and eventually render the CM model unstable. The appearance of these unrealistic oscillations, well reported in the literature, are related to the neglected influence of the local bed-slope on the bedload transport, which would otherwise introduce diffusion into the bed-update equation, preventing such oscillations from developing (Johnson & Zyserman 2002). The Q2L model captures correctly the qualitative behaviour of the hump as it migrates downstream, i.e. steepening of its downstream face with time. However, in contrast with the CM model, high-frequency oscillations are not present in the hump, thus stabilising the model and permitting

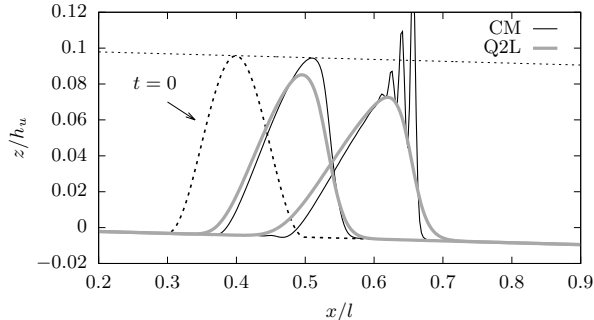


FIGURE 9. Time evolution (from left to right) of a hump predicted by the CM and Q2L models.

longer simulations to be carried out (see Fig. 10). This is most likely due to an inherent diffusive component within the model that prevents small perturbations from forming. This theory is supported by the fact that the hump losses height with time (diffusive behaviour). It is suggested (e.g. Johnson & Zyserman 2002) that this diffusion (or smoothing effect) is related and proportional to the local bed-slope. To further explore this hypothesis, Fig 10 illustrates the evolution of the hump profile predicted by the Q2L model for a longer simulation ($1.2 \times 10^6 \text{s} \approx 14 \text{ days}$). The height of the hump converges with time, thus supporting the idea that the diffusion component of the model vanishes for small local slopes, and hence, that such diffusion is indeed proportional to the bed-slope. Note that, although to the authors' knowledge no high-quality measurements are available on the exact diffusion that an erodible sandbar presents under the conditions herein studied, inclusion of bed-slope-related diffusion in a morphological model is underpinned by phenomenological observations in field and laboratory (e.g Castro Díaz *et al.* 2008; Moulton *et al.* 2014), and should thus not be interpreted as an auxiliary tool whose sole target is to avoid oscillations arising from the numerical technique employed (for numerical strategies aimed at preventing such oscillations see e.g. Callaghan *et al.* 2006; Hudson & Sweby 2003; Johnson & Zyserman 2002). It is here hypothesised that the Q2L model accounts inherently for the bed-slope-related influence on bedload and morphological evolution. Such a hypothesis is explored in detail by Maldonado-Villanueva (2015).

7. Conclusions

A physics-based Quasi-2-Layer model for predicting sediment transport rates and morphological evolution has been introduced. The model has the main advantages of reducing the degree of empiricism common to most conventional morphodynamic models by not requiring an empirical formula for transport rates (out of a vast catalogue of options) to achieve closure, and accounting naturally for the ambiguity in the distinction between bedload and total load by setting an arbitrary vanishing thickness ($\sim D$) of the bedload layer. Model results are weakly dependent on such arbitrary selection within the range of values studied; a value of $h_0 \approx 10D$ is recommended. The model can simulate three modes of transport: no sediment transport at all, bedload only, and total load. The model can be tuned either from hydrodynamic data or by comparing its results against information on sediment transport rates. We show that both approaches yield mutually consistent estimates of the tuning parameters, $c^{(b)}$ and $c^{(i)}$. Predicted bedload transport rates solely depend on $c^{(b)}$, whereas total load is dependent on both

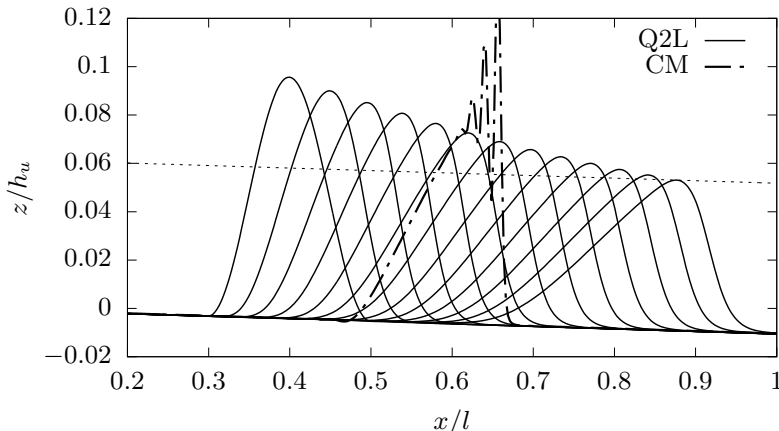


FIGURE 10. Evolution of a hump predicted by the Q2L model after 1.2×10^6 s illustrating hump height convergence with time. Results shown every 100×10^3 s. CM model superimposed, showing physically unrealistic prediction. Dotted straight line is tangent to the final crest of the hump (parallel to the otherwise flat bed).

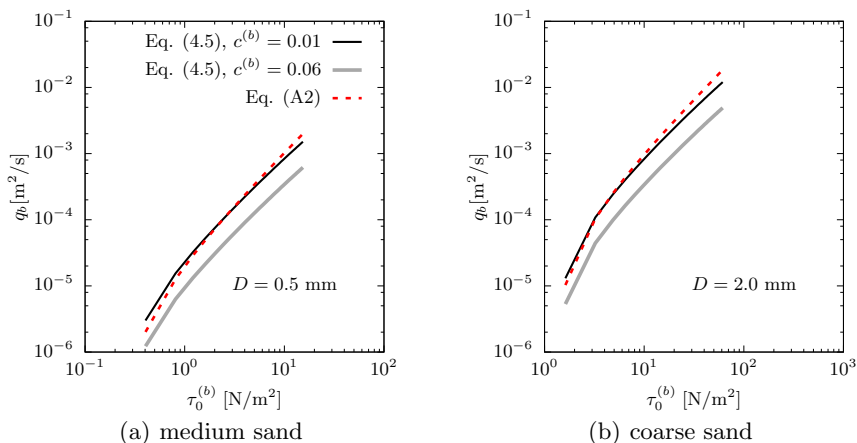


FIGURE 11. Comparison between dimensional bedload predicted by $q_b = f(u_{s0})$ (eq. A2) and $q_b = f(u_0)$ (eq. 4.5) for two values of $c^{(b)}$ and for two different particle diameters.

$c^{(b)}$ and $c^{(z)}$ (the ratio $c^{(b)}/c^{(z)}$ may be estimated from the hydrodynamic calibration; see Fig. 5). The model has been satisfactorily validated against empirical expressions for bedload and total load. Analytical solutions to the model have been derived for the three modes of transport, for the case of a steady uniform flow over an erodible bed. These solutions provide a powerful tool to analyse the model in depth. For example, use of the model to estimate the thickness of a sheet transport layer agrees with previous approaches, the model agrees mathematically with well-known empirical formulae for bedload and within the present framework, conflicting views about the behaviour of shear stress under sediment-transport conditions appear to reconcile. The Q2L model has also been compared against a conventional morphodynamic model for the case study of a migrating submerged hump (sandbar) subject to a steady subcritical current. The proposed model outperforms the conventional approach by naturally suppressing the

appearance of spurious oscillations, while predicting the correct qualitative evolution of the hump (steepening of its lee while migrating downstream), hence stabilising the code and permitting longer-term simulations. A conventional model would require additional mathematical or numerical treatment in order to avoid such unrealistic instabilities. Potential improvements of the model include the addition of non-uniform sediment and a parameter study of key variables, such as $c^{(b)}$, $\tau_b^{(b)}$, τ_c and $\tau_0^{(b)}$.

The first author was supported by the Mexican National Council for Science and Technology (CONACyT) through scholarship No. 310043 and the Mexican Ministry of Education (SEP). The first author would also like to thank the University of Edinburgh, where he was based when much of this work was undertaken.

Appendix A

In order to study the relationship between the stream-wise velocity of the sediment bedload particles and that of the bedload (water-sediment mixture) layer, an expression of the form $u_{s0}/u_* = \hat{a} + \hat{b} \ln D_* - \hat{c} T_*^{-1/2}$ (van Rijn 1984a; Engelund & Hansen 1967) is employed; where \hat{a} , \hat{b} and \hat{c} are tuning parameters; $D_* \equiv D[(s-1)g/\nu^2]^{1/3}$ is the non-dimensional particle diameter, with s and ν being the sediment density relative to water and water kinematic viscosity, respectively; u_* is the bed friction velocity; and $T_* \equiv \tau_0^{(b)}/\tau_c$ is the transport stage. Considering that $\tau = \rho_w u_*^2 = \tau_0^{(b)} = \rho_0 c^{(b)} u_0^2$, the stream-wise bedload particle velocity for a given particle diameter can be written as:

$$u_{s0} = \hat{d} \left(\frac{\rho_0 c^{(b)}}{\rho_w} \right)^{1/2} u_0 - \hat{c} \left(\frac{\tau_c}{\rho_w} \right)^{1/2}, \quad (\text{A } 1)$$

where $\hat{d} = \hat{a} + \hat{b} \ln D_*$. Hence, invoking (4.3) in order to compute $q_b = h_0 c_0 u_{s0}$ and using the substitution $u_0 = \sqrt{\tau_0^{(b)}/c^{(b)}}$, yields

$$q_b = \frac{(\tau_0^{(b)} - \tau_c)}{(\rho_s - \rho_w)g \tan \varphi} \left[\hat{d} \left(\frac{\tau_0^{(b)}}{\rho_w} \right)^{1/2} - \hat{c} \left(\frac{\tau_c}{\rho_w} \right)^{1/2} \right]. \quad (\text{A } 2)$$

Note that the above equation follows the form of expressions for bedload proposed by Ashida & Michue (1972) and Madsen (1991). It is worth observing that, unlike the solution derived in §4.1 (eq. 4.5), the above equation does not depend on $c^{(b)}$ nor h_0 ; however, values of \hat{c} and \hat{d} have to be set instead for calibration. Based on numerical experiments within a Lagrangian framework, Maldonado & Borthwick (2015) found values of $\hat{d} = 8.328 + 1.328 \ln D_*$ and $\hat{c} = 6.232$. Fig. 11 compares the bedload rate predicted by (A 2), using the aforementioned values of the coefficients, against the analytical solution derived in §4.1 (eq. 4.5). Two particle diameters are considered. Fig. 11 confirms that the results and analysis presented throughout this paper for the Q2L model, based on the assumption $u_0 = u_{s0}$, appear valid from a practical viewpoint. It can be observed that for $c^{(b)} \approx 0.01$, both expressions yield very similar results. However, this is only the case for the considered values of calibration coefficients \hat{a} , \hat{b} and \hat{c} , which result from the particular ranges of particle diameter and flow velocity investigated by Maldonado & Borthwick (2015).

REFERENCES

- ABBOTT, M.B. 1979 *Computational Hydraulics: Elements of the Theory of Free Surface Flows*. Great Britain: Ashgate.
- ACKERS, PETER & WHITE, WILLIAM R. 1973 Sediment transport: new approach and analysis. *Journal of the Hydraulics Division* **99**.
- AMOUDRY, LAURENT O. & SOUZA, ALEJANDRO J. 2011 Deterministic coastal morphological and sediment transport modeling: A review and discussion. *Reviews of Geophysics* **49** (2010), 1–21.
- ARMANINI, ARONNE & DI SILVIO, GIAMPAOLO 1988 A one-dimensional model for the transport of a sediment mixture in non-equilibrium conditions. *Journal of Hydraulic Research* **26**, 275–292.
- ASHIDA, KAZUO & MICHUE, M. 1972 Study on hydraulic resistance and bed-load transport rate in alluvial streams. *Journal of Civil Engineering, Jpn Soc Civil Engineers* **206**, 59–69.
- BAGNOLD, R. A. 1956 The Flow of Cohesionless Grains in Fluids. *Philosophical Transactions of the Royal Society A: Mathematical, Physical and Engineering Sciences* **249** (964), 235–297.
- BAGNOLD, R. A. 1963 Mechanics of marine sedimentation. In *The sea* (ed. M. N. Hill), , vol. 3. Great Britain: Interscience Publishers.
- BAKHTYAR, ROHAM, YEGANEH-BAKHTIARY, ABBAS, BARRY, DAVID ANDREW & GHAHERI, ABBAS 2009 Two-phase hydrodynamic and sediment transport modeling of wave-generated sheet flow. *Advances in Water Resources* **32** (8), 1267–1283.
- CALLAGHAN, DAVID P., SAINT-CAST, FRÉDÉRIC, NIELSEN, PETER & BALDOCK, TOM E. 2006 Numerical solutions of the sediment conservation law; a review and improved formulation for coastal morphological modelling. *Coastal Engineering* **53**, 557–571.
- CAMENEN, BENOÎT & LARROUDÉ, PHILIPPE 2003 Comparison of sediment transport formulae for the coastal environment. *Coastal Engineering* **48**, 111–132.
- CAPART, H & YOUNG, DL 1998 Formation of a jump by the dam-break wave over a granular bed. *Journal of Fluid Mechanics* **372**, 165–187.
- CASTRO DÍAZ, M. J., FERNÁNDEZ-NIETO, E. D. & FERREIRO, A. M. 2008 Sediment transport models in Shallow Water equations and numerical approach by high order finite volume methods. *Computers & Fluids* **37**, 299–316.
- DISSANAYAKE, D. M P K, ROELVINK, J. A. & VAN DER WEGEN, M. 2009 Modelled channel patterns in a schematized tidal inlet. *Coastal Engineering* **56** (11-12), 1069–1083.
- EINSTEIN, H A 1950 The bed-load function for sediment transport in open channel flows. *Agriculture. Soil Conservation Service. Tech. Bull* **1026**.
- ENGELUND, FRANK & HANSEN, EGGERT 1967 A monograph on sediment transport in alluvial streams. *Tech. Rep.. TEKNISKFORLAG Skelbreggade 4 Copenhagen V, Denmark*.
- FANG, HONG-WEI & WANG, GUANG-QIAN 2000 Three-Dimensional Mathematical Model of Suspended-Sediment Transport. *Journal of Hydraulic Engineering* **126** (8), 578–592.
- FERNÁNDEZ LUQUE, R. & VAN BEEK, R. 1976 Erosion And Transport Of Bed-Load Sediment. *Journal of Hydraulic Research* **14** (October 2014), 127–144.
- FRACCAROLLO, L. & CAPART, H. 2002 Riemann wave description of erosional dam-break flows. *Journal of Fluid Mechanics* **461**, 183–228.
- FREDSØE, J. & DEIGAARD, R. 1992 *Mechanics of Coastal Sediment Transport, Advanced series on ocean engineering*, vol. 3. Singapore: World Scientific.
- GARNIER, R., CALVETE, D., FALQUÉS, A. & CABALLERIA, M. 2006 Generation and nonlinear evolution of shore-oblique/transverse sand bars. *Journal of Fluid Mechanics* **567**, 327.
- GOMEZ, BASIL & CHURCH, MICHAEL 1989 An assessment of bed load sediment transport formulae for gravel bed rivers. *Water Resources Research* **25** (6), 1161.
- GRECO, MASSIMO, IERVOLINO, MICHELE, LEOPARDI, ANGELO & VACCA, ANDREA 2013 A two-phase model for fast geomorphic shallow flows. *International Journal of Sediment Research* **27** (4), 409–425.
- HUANG, JINGMIN, BORTHWICK, ALISTAIR G. L. & SOULSBY, RICHARD L. 2008 One-dimensional modelling of fluvial bed morphodynamics. *Journal of Hydraulic Research* **46** (5), 636–647.
- HUDSON, JUSTIN & SWEBY, PETER K. 2003 Formulations for Numerically Approximating Hyperbolic Systems Governing Sediment Transport. *Journal of Scientific Computing* **19** (December), 225–252.

- JOHNSON, HAKEEM K. & ZYSERMAN, JULIO A. 2002 Controlling spatial oscillations in bed level update schemes. *Coastal Engineering* **46**, 109–126.
- KOVACS, AGNES & PARKER, GARY 1994 A new vectorial bedload formulation and its application to the time evolution of straight river channels. *Journal of Fluid Mechanics* **267**, 153.
- LI, JI, CAO, ZHIXIAN, PENDER, GARETH & LIU, QINGQUAN 2013 A double layer-averaged model for dam-break flows over mobile bed. *Journal of Hydraulic Research* **51**, 518–534.
- MADSEN, OLE SECHER 1991 Mechanics of cohesionless sediment transport in coastal waters. In *Coastal Sediments (1991)*, pp. 15–27. ASCE.
- MALDONADO, SERGIO & BORTHWICK, ALISTAIR G L 2015 Sensitivity Analysis and Statistical Convergence of a Saltating Particle Model. *Journal of Hydraulic Engineering* **141** (5), 04014091.
- MALDONADO-VILLANUEVA, SERGIO 2015 Quasi 2-Layer Morphodynamic Model and Lagrangian Study of Bedload. PhD thesis, The University of Edinburgh, Edinburgh, U.K.
- MEYER-PETER, E. & MÜLLER, R. 1948 Formulas for Bed-Load Transport. *International Association for Hydraulic Structures Research - Zweite Tagung - Second meeting - Deuxième réunion*.
- MOULTON, MELISSA, ELGAR, STEVE & RAUBENHEIMER, BRITT 2014 A surfzone morphological diffusivity estimated from the evolution of excavated holes. *Geophysical Research Letters* **41**.
- NI, J. R., WANG, G. Q. & BORTHWICK, A. G. L. 2000 Kinetic Theory for Particles in Dilute and Dense Solid-Liquid Flows. *Journal of Hydraulic Engineering* **126** (12), 893–903.
- NIÑO, YARKO & GARCÍA, MARCELO 1998 Using Lagrangian particle saltation observations for bedload sediment transport modelling. *Hydrological Processes* **12**, 1197–1218.
- NIELSEN, PETER 1992 *Coastal bottom boundary layers and sediment transport*, vol. 4. World scientific.
- NNADI, FIDELIA N. & WILSON, KENNETH C 1992 Motion of Contact-Load Particles at High Shear Stress. *Journal of Hydraulic Engineering* **118** (12), 1670–1684.
- PARKER, GARY, SEMINARA, GIOVANNI & SOLARI, LUCA 2003 Bed load at low Shields stress on arbitrarily sloping beds: Alternative entrainment formulation. *Water Resources Research* **39** (7), 1–11.
- PUGH, FRANÇOIS J & WILSON, KENNETH C 1999 Velocity and concentration distributions in sheet flow above plane beds. *Journal of Hydraulic Engineering* **125** (2), 117–125.
- RIBBERINK, JAN S & AL-SALEM, ABDULLAH A 1994 Sediment transport in oscillatory boundary layers in cases of rippled beds and sheet flow. *Journal of Geophysical Research: Oceans (1978–2012)* **99** (C6), 12707–12727.
- ROSATTI, G. & FRACCAROLLO, L. 2006 A well-balanced approach for flows over mobile-bed with high sediment-transport. *Journal of Computational Physics* **220**, 312–338.
- SEMINARA, GIOVANNI, SOLARI, LUCA & PARKER, GARY 2002 Bed load at low Shields stress on arbitrarily sloping beds: Failure of the Bagnold hypothesis. *Water resources research* **38** (11), 31–1.
- SOULSBY, RICHARD 1997 *Dynamics of Marine Sands: A Manual for Practical Applications*. Great Britain: Thomas Telford.
- SOULSBY, RICHARD L. & DAMGAARD, JESPER S. 2005 Bedload sediment transport in coastal waters. *Coastal Engineering* **52**, 673–689.
- SPINEWINE, B. 2005 Two-layer flow behaviour and the effects of granular dilatancy in dam-break induced. PhD thesis, Université catholique de Louvain, Louvain-la-Neuve, Belgium.
- VAN EMELLEN, SYLVIE, ZECH, YVES & SOARES-FRAZÃO, SANDRA 2015 Impact of sediment transport formulations on breaching modelling. *Journal of Hydraulic Research* **53** (1), 60–72.
- VAN RIJN, LEO C. 1984a Sediment transport, part I: bed load transport. *Journal of Hydraulic Engineering* **110** (10), 1431–1456.
- VAN RIJN, LEO C. 1984b Sediment transport, part II: suspended load transport. *Journal of hydraulic engineering* **110** (11), 1613–1641.
- WILSON, KENNETH C 1966 Bed-load transport at high shear stress. *Journal of the Hydraulics Division* **92** (6), 49–59.
- WILSON, KENNETH C. 1987 Analysis of Bed-Load Motion at High Shear Stress. *Journal of Hydraulic Engineering* **113** (1), 97–103.

- YALIN, M SELIM 1963 An expression for bed-load transportation. *Journal of the Hydraulics Division* **89** (3), 221–250.
- YANG, CHIH TED & WAN, SCHENGGAN 1991 Comparisons of Selected Bed-Material Load Formulas. *Journal of Hydraulic Engineering* **117** (8), 973–989.
- YANG, SHU-QING, TAN, SOON-KEAT & LIM, SIOW-YONG 2004 Velocity Distribution and Dip-Phenomenon in Smooth Uniform Open Channel Flows. *Journal of Hydraulic Engineering* **130** (12), 1179–1186.
- ZECH, Y., SOARES-FRAZÃO, S., SPINOWINE, B. & LE GRELE, N. 2008 Dam-break induced sediment movement: Experimental approaches and numerical modelling. *Journal of Hydraulic Research* **46**, 176–190.